remote sensing

MDPI

Communication

DOA Estimation under GNSS Spoofing Attacks Using a Coprime Array: From a Sparse Reconstruction Viewpoint

Yuqing Zhao [1], Feng Shen [1,*], Biqing Qi [2] and Zhen Meng [3]

[1] School of Instrumentation Science and Engineering, Harbin Institute of Technology, Harbin 150001, China
[2] School of Astronautics, Harbin Institute of Technology, Harbin 150001, China
[3] School of Information and Control Engineering, China University of Mining and Technology, Xuzhou 221116, China
* Correspondence: fshen@hit.edu.cn

Abstract: The antispoofing method using the direction-of-arrival (DOA) feature can effectively improve the application security of the global navigation satellite system (GNSS) receivers. In this paper, a sparse reconstruction approach based on a coprime array of antennas is proposed to provide reliable DOA estimation under a GNSS spoofing attack. Specifically, the self-coherence property of genuine satellite signals and spoofing was fully exploited to construct a denoised covariance matrix that enables DOA estimation before receiver despreading. Based on this, an equivalent uniform linear array (ULA) was generated from the constructed covariance matrix via virtual array interpolation. By applying the ideal of sparse reconstruction to an equivalent ULA signal, the preliminary DOA estimation results could be obtained without the need for a number of signals. Considering that the sparse estimation technique suffers from basis mismatch effects, we designed an optimization problem with respect to off-grid error to compensate the initial DOA such that the performance loss of DOA estimation could be reduced. Numerical examples demonstrated the advantages of the proposed method in terms of degrees-of-freedom (DOFs), resolution and accuracy.

Keywords: GNSS; antispoofing; DOA estimation; coprime array; sparse reconstruction

Citation: Zhao, Y.; Shen, F.; Qi, B.; Meng, Z. DOA Estimation under GNSS Spoofing Attacks Using a Coprime Array: From a Sparse Reconstruction Viewpoint. *Remote Sens.* **2022**, *14*, 5944. https://doi.org/10.3390/rs14235944

Academic Editors: Mohammad Zahidul Hasan Bhuiyan and Elena Simona Lohan

Received: 24 October 2022
Accepted: 21 November 2022
Published: 24 November 2022

1. Introduction

A spoofing attack is an intelligent GNSS-like interference that coerces a victim receiver into providing false position/navigation information, which could lead to disastrous consequences in civil and military applications [1,2]. As such, several spoofing detection and mitigation techniques have been proposed to defend against this type of interference [3]. The spatial countermeasure based on antenna arrays is considered one of the most powerful approaches among them [4]. In particular, the DOA feature provided by antenna arrays plays an important role in both spoofing detection and suppression [5,6].

The discussions in [7] indicate that the performance of DOA estimation in the spoofing environment should be improved to reliably detect and suppress spoofing signals. However, to the best of the authors' knowledge, little has been written about DOA estimation under a spoofing attack in the open literature. To identify the GNSS signals (including spoofing and real signals) from raw signal samples, the cyclic music signal classification (Cyclic-MUSIC) method was utilized in [6] for DOA estimation before the despreading of receivers. The work of [8] was concerned with DOA estimation for GNSS signals under a spoofing attack and a multipath environment, where the rank recovery algorithm was adopted to reduce the strong correlation between incident signals. Considering in the "underdetermined" case that the number of GNSS signals is more than the number of sensors in the antenna array, the conventional algorithms in the paper [6,8] are no longer in force due to the use of the uniform antenna array. In recent years, emerging sparse array structures, such as the coprime array and the generalized coprime array, have attracted noticeable attention in DOA estimation because of their superior estimation performance to the uniform array [9,10]. In paper [11], an L-shaped sparse array was introduced into the EMVS-MIMO radar, and a fast, accurate and DOF enhanced two-dimensional parameter estimation method was designed. Therefore, it seems that a sparse array might also be beneficial for improving the estimation performance of GNSS signal parameters. Inspired by this, in earlier works we proposed an underdetermined DOA estimation technology based on the sparse coprime array for GNSS signals, where the achievable DOFs could be increased by deriving an extended virtual array [12]. Nevertheless, the scheme in [12] fails to make full use of all the elements contained in the virtual array, which dramatically affects the estimation performance under a spoofing attack. In addition, the DOA estimation problems in [6,8,12] were solved by classical subspace-based methods; they required the number of incident signals to be prespecified or estimated [13]. In this sense, it is of great importance to achieve better DOA estimation performance in the GNSS spoofing environment without using the number of signals as a priori information.

To this end, we proposed a novel coprime array-based algorithm that adopts the sparse recovery technique for DOA estimation under a GNSS spoofing attack. Unlike previous methods in [6,8,12], our method combines virtual array interpolation and off-grid error compensation to obtain better estimation performance, and it does not require a pre-estimation of the number of incident sources. Notably, the proposed method takes advantage of the raw digital baseband signal, hence it can identify authentic signals and spoofing before the despreading stage of the receiver, which avoids signal acquisition, tracking and the position solution. In order to fully exploit all information provided by the derived virtual array, we constructed an equivalent ULA signal through the array interpolation method. Based on this, the suggested algorithm employs sparse reconstruction technology to the equivalent signal. Since the DOAs of spoofing and authentic satellite signals are unlikely to lie on the predefined spatial grid, the sparse-based approach is subject to basis mismatch effects [13,14]. In view of this, we formulated it as an optimization problem with respect to off-grid error, thereby the estimation error caused by the predefined grid could be iteratively compensated.

The main contributions of this paper can be categorized as follows:

- We suggest a coprime array-based method from a sparse reconstruction perspective to estimate the DOA of GNSS signals in the spoofing environment.
- The scheme combines virtual array interpolation with the proposed off-grid error compensation technology to provide better DOA estimation performance, which is beneficial to subsequent spoofing detection and suppression.
- Our approach not only does not need to know the number of incident GNSS signals in advance, but also can estimate the DOAs of spoofing and real signals before receiver despreading.

The rest of the paper is organized as follows. In Section 2, we first introduce the signal model of the coprime array in the GNSS spoofing environment. Then, we elaborate the designed sparse recovery-based DOA estimation algorithm under a spoofing attack in Section 3. After that, we provide numerical simulations in Section 4 to validate the advantages of our method. Finally, the conclusions are given in Section 5.

Notations: lower-case and upper-case boldface characters are used to denote vectors and matrices, respectively; $(\cdot)^T$, $(\cdot)^*$ and $(\cdot)^H$ stand for the transpose, conjugation and Hermitian transpose, respectively; $\|\cdot\|_F$ denotes the Frobenius norm; $\|\cdot\|_0$ and $\|\cdot\|_2$ are, respectively, the l_0 norm and l_2 norm; $E\{\cdot\}$ and $vec(\cdot)$ represent the expectation operator and vectorization operator, respectively; the symbol $\otimes$ means the Kronecker product; $[\cdot]_{i,j}$ denotes the element in the i-th row and the j-th column of a matrix; $|S|$ is the cardinality of a set S; the functions $rank(\cdot)$ and $Tr(\cdot)$ represent the rank and trace of the matrix, respectively; $\succeq$ is matrix inequality; and $\Re\{\cdot\}$ means the real part of a complex variable.

2. Signal Model

In this paper, we suppose that the spoofing attack contains L^S counterfeit PRN signals, which are transmitted from a single antenna, and there are L^A authentic signals incident on the extended coprime array. The discretized received signal vector $x(n)$ at snapshot n can be modeled as

$$\boldsymbol{x}(n) = \boldsymbol{s}^A(n) + \boldsymbol{s}^S(n) + \boldsymbol{n}(n) \tag{1}$$

in which $\boldsymbol{s}^A(n) = \sum_{l=1}^{L^A} \boldsymbol{a}(\theta_l)s_l(n)$ and $\boldsymbol{s}^S(n) = \sum_{l=1}^{L^S} \boldsymbol{a}(\theta_s)s'_l(n)$ are the real signal component and the spoofing component, respectively, and $n(n)$ is the additive white Gaussian noise component. The $s'_l(n)$ and $s_l(n)$ denote waveforms of the l-th spoofing and the l-th real signal, respectively. The variables $\boldsymbol{a}(\theta_s)$ and $\boldsymbol{a}(\theta_l)$ in Equation (1) are the steering vectors of the spoofing and the l-th authentic signal, respectively, which can be expressed as

$$\boldsymbol{a}(\theta) = \left[1, \cdots, e^{-j\frac{2\pi}{\lambda}d_i \sin\theta}, \cdots, e^{-j\frac{2\pi}{\lambda}d_{2M_1+M_2-1}\sin\theta}\right]^T \tag{2}$$

where the parameter λ is the wavelength of the GNSS signals, $\theta = [\theta_1, \theta_2, \cdots, \theta_{L^A}, \theta_s]$ represents the spatial direction of the incident signals and $d_i(i = 1, \cdots, 2M_1 + M_2 - 1)$ denotes the position of the antenna in the extended coprime array, which are shown in Figure 1. As Figure 1 shows, the extended coprime array consists of a pair of ULAs with $2M_1$ and M_2 elements, whose antennas are respectively located at $\{0, M_1d, 2M_1d, \cdots, (M_2 - 1)M_1d\}$ and $\{0, M_2d, 2M_2d, \cdots, (2M_1 - 1)M_2d\}$. Here, $d = \lambda/2$, M_1 and M_2 are coprime integers.

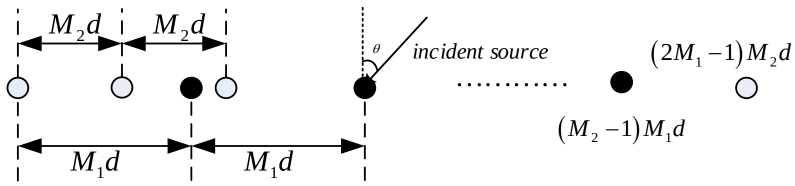

Figure 1. Extended coprime array configuration.

3. Proposed DOA Estimation Method under a Spoofing Attack

3.1. Noise Component Suppression

Due to the fact that spoofing signals and real satellite signals are buried under the noise floor in the raw signal samples, it is a challenge to identify the direction of incoming signals before receiver despreading. In order to overcome this problem, we employed the cyclostationary property [15] of the GNSS signals (including genuine and spoofing signals) to suppress the noise components in the data covariance matrix. We first obtained the reference data $\boldsymbol{x}_G(n)$ corresponding to the data vector $\boldsymbol{x}(n)$ as follows:

$$\begin{aligned} \boldsymbol{x}_G(n) &= \boldsymbol{s}^A(n - jG) + \boldsymbol{s}^S(n - jG) + \boldsymbol{n}(n - jG) \\ &= \boldsymbol{s}^A(n) + \boldsymbol{s}^S(n) + \boldsymbol{n}(n - jG) \end{aligned} \tag{3}$$

in which jG is the distance between the respective samples in $\boldsymbol{x}(n)$ and $\boldsymbol{x}_G(n)$. In this paper, we take GPS C/A signal as an example, hence we have the spreading gain $G = 1023$ and $1 \le j < 20$ [16]. Then, the covariance matrix between $\boldsymbol{x}(n)$ and $\boldsymbol{x}_G(n)$ can be given by

$$\begin{aligned} \boldsymbol{R}_x^{(G)} &= E\left\{\boldsymbol{x}(n)\boldsymbol{x}_G{}^H(n)\right\} = \boldsymbol{R}_s + \boldsymbol{R}_n \\ &= E\left\{\left[\boldsymbol{s}^A(n) + \boldsymbol{s}^S(n)\right]\left[\boldsymbol{s}^A(n) + \boldsymbol{s}^S(n)\right]^H\right\} \\ &= \sum_{l=1}^{L^A} \boldsymbol{a}(\theta_l)\boldsymbol{a}^H(\theta_l)\boldsymbol{R}_{s_l s_l} + \sum_{l=1}^{L^S} \boldsymbol{a}(\theta_s)\boldsymbol{a}^H(\theta_s)\boldsymbol{R}_{s'_l s'_l} \end{aligned} \tag{4}$$

where $\boldsymbol{R}_s = E\left\{\left[\boldsymbol{s}^A(n) + \boldsymbol{s}^S(n)\right]\left[\boldsymbol{s}^A(n) + \boldsymbol{s}^S(n)\right]^H\right\}$ and $\boldsymbol{R}_n = E\{\boldsymbol{n}(n)\boldsymbol{n}^H(n - jG)\}$. As a result of Gaussian white noise $\boldsymbol{n}(n)$, we have $\boldsymbol{R}_n = 0$. In Equation (4), $\boldsymbol{R}_{s_l s_l} = E\left\{s_l(n)s_l(n)^H\right\}$

and $\boldsymbol{R}_{s'_l s'_l} = E\left\{ s'_l(n) s'_l(n)^H \right\}$. We adopted the sampling covariance matrix $\hat{\boldsymbol{R}}^{(G)}$ to replace $\boldsymbol{R}_x^{(G)}$ in practice, and $\hat{\boldsymbol{R}}^{(G)}$ can be denote as

$$\hat{\boldsymbol{R}}_x^{(G)} \approx \frac{1}{N} \boldsymbol{X}_N \boldsymbol{X}_{ref}^H \tag{5}$$

where $\boldsymbol{X}_N = [\boldsymbol{x}(n) \cdots \boldsymbol{x}(n-(N-1))]$ and $\boldsymbol{X}_{ref} = [\boldsymbol{x}_G(n) \cdots \boldsymbol{x}_G(n-(N-1))]$ are the data block and the reference data block, respectively. The parameter N denotes the length of samples in the data/reference data block.

3.2. Array Interpolation and Matrix Recovery

To make full use of the maximum aperture provided by the virtual array, which is derived from the data covariance matrix, we constructed an equivalent ULA signal in this subsection via the array interpolation technique. In detail, we first vectorized $\boldsymbol{R}_x^{(G)}$, that is

$$\boldsymbol{z} = vec(\boldsymbol{R}_x^{(G)}) = \boldsymbol{B}\boldsymbol{p} \tag{6}$$

where $\boldsymbol{p} = \left[\boldsymbol{R}_{s_1 s_1}, \boldsymbol{R}_{s_2 s_2}, \cdots \boldsymbol{R}_{s_{L^A} s_{L^A}}, \sum_{l=1}^{L^S} \boldsymbol{R}_{s'_l s'_l} \right]^T$ and

$$\boldsymbol{B} = [\boldsymbol{a}^*(\theta_1) \otimes \boldsymbol{a}(\theta_1), \cdots \boldsymbol{a}^*(\theta_{L^A}) \otimes \boldsymbol{a}(\theta_{L^A}), \boldsymbol{a}^*(\theta_s) \otimes \boldsymbol{a}(\theta_s)]. \tag{7}$$

Then, we removed the repeated elements in $\boldsymbol{B}$ and acquired an equivalent virtual signal with an increased number of DOFs, which can be denoted as

$$\boldsymbol{z}_v = \boldsymbol{B}_v \boldsymbol{p} \tag{8}$$

where $\boldsymbol{B}_v$ is the steering matrix of the virtual array S_v. For the extended coprime array geometry shown in Figure 1, the position of the virtual sensors in S_v can be calculated by

$$\begin{aligned} S_v = \{\pm(M_1 m_2 - M_2 m_1) | m_1 &= 0, d, 2d, \cdots (2M_1 - 1)d \\ m_2 &= 0, d, 2d, \cdots (M_2 - 1)d\} \end{aligned} \tag{9}$$

Figure 2 adopts the extended coprime array geometry with $M_1 = 3$ and $M_2 = 5$ as an example to illustrate the concept intuitively. Owing to several missing elements, the derived virtual array S_v shown in Figure 2b is nonuniform. In this situation, the traditional ULA-based DOA estimation methods are not available. To overcome this challenge, a common solution is to ditch the discontinuous elements and select only the largest contiguous virtual sensors in S_v for subsequent processing [17]. However, this method suffers from performance degradation since the elements offered by S_v cannot be fully utilized.

Consequently, we employ array interpolation technology in this paper to fill the discontinuous sensors in S_v. Obviously, the interpolated virtual ULA S_I shown in Figure 2c has $2M_2(2M_1-1)+1$ elements in total, the signal of S_I can be initialized as

$$[\boldsymbol{z}_I]_i = \begin{cases} [\boldsymbol{z}_v]_i & i \in S_v \\ 0 & i \in S_I - S_v \end{cases} \tag{10}$$

where $[\cdot]_i$ is the virtual element at the i-th position. Considering the signal at each interpolated sensor is assumed to be zero in Equation (10), it is necessary to recover the unknown information in z_I. According to the relationship established in [18], the Toeplitz covariance matrix of the interpolated virtual signal z_I can be constructed by

$$R_v = \begin{bmatrix} \langle z_I \rangle_{L_I} & \langle z_I \rangle_{L_I - 1} & \cdots & \langle z_I \rangle_1 \\ \langle z_I \rangle_{L_I + 1} & \langle z_I \rangle_{L_I} & \cdots & \langle z_I \rangle_2 \\ \vdots & \vdots & \ddots & \vdots \\ \langle z_I \rangle_{2L_I - 1} & \langle z_I \rangle_{2L_I - 2} & \cdots & \langle z_I \rangle_{L_I} \end{bmatrix} \tag{11}$$

where $\langle z_I \rangle_i$ denotes the i-th element in z_I, and $L_I = (|S_I| + 1)/2$.

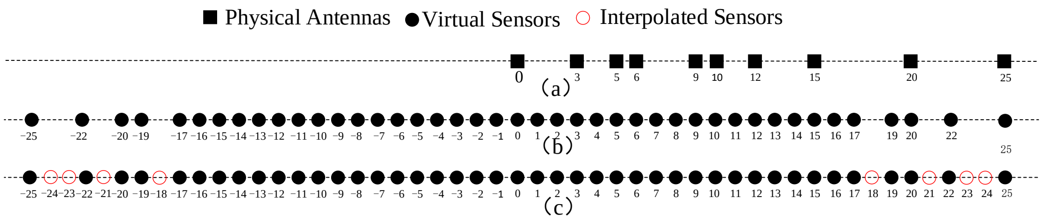

Figure 2. Various array representations are given with $M_1 = 3$ and $M_2 = 5$. (**a**) Extended coprime array; (**b**) virtual array S_v; (**c**) interpolated virtual array S_I.

Taking R_v in Equation (11) as the reference, the rank minimization problem of the R_v reconstruction can be formulated as

$$\begin{gathered} \hat{z} = \arg\min rank(R(z)) \\ \text{subject} \quad \text{to} \|M_P(R(z)) - R_v\|_F^2 < \varepsilon, R(z) \succeq 0 \end{gathered} \tag{12}$$

where ε is the predefined threshold-of-fitting error. The elements of $M_P(R(z))$ can be obtained by the product of the corresponding elements in $R(z)$ and P. Matrix $R(z)$ has an Hermitian Toeplitz form, and its first column is the optimization variable z. If P is a binary matrix, the elements in it can be defined as

$$[P]_{i,j} = \begin{cases} 0 & [R_v]_{i,j} = 0 \\ 1 & else \end{cases} \tag{13}$$

Due to the rank function, the optimization problem in (12) is an NP-hard problem. To solve this problem, we reformulate it by introducing a trace function $Tr(\cdot)$, thus we have

$$\begin{gathered} \hat{z} = \arg\min \tfrac{1}{2} \|M_P(R(z)) - R_v\|_F^2 + \mu Tr(R(z)) \\ \text{subject} \quad \text{to} \quad R(z) \succeq 0 \end{gathered} \tag{14}$$

where μ denotes the regularization parameter, which is used to balance the trace of $R(z)$ and the fitting error. Now, the optimization problem (14) is convex, which can be efficiently solved to obtain the optimum solution $\hat{z}$ and its corresponding $T(\hat{z})$ [19].

3.3. Off-Grid DOA Estimation

In this subsection, we first perform sparse reconstruction technology on the interpolated virtual signal $\hat{z}$ to obtain the initial DOA estimation results, which can be formulized as

$$\hat{p} = \arg\min_{p} \|p\|_0 \quad \text{subject} \quad \text{to} \|\hat{z} - B_I p\|_2 < \varepsilon \tag{15}$$

where B_I is the steering matrix of the interpolated virtual array S_I with $2M_2(2M_1 - 1) + 1$ elements and the k-th column of B_I can be given by

$$a(\theta_k) = \left[1, \cdots, e^{-j\frac{2\pi}{\lambda} d_i \sin\theta_k}, \cdots, e^{-j\frac{2\pi}{\lambda} d_{2M_2(2M_1-1)+1} \sin\theta_k}\right]^T \tag{16}$$

The optimization spatial spectrum $\hat{\boldsymbol{p}}$ in Equation (15) can be acquired by the LASSO algorithm [20] through a prespecified spatial grid. By searching peaks of $\hat{\boldsymbol{p}}$, the initial DOA results $\hat{\theta}_k^l (l = 1, 2, \cdots, K)$ can be estimated. Meanwhile, the number of incoming signals K is revealed as a by-product without additional estimation.

Although we make full use of the maximum aperture provided by the virtual array to estimate the initial DOAs, the estimation performance is affected by the basis mismatch effect since the actual DOAs are unlikely to be located at the prespecified grids. In view of this, an off-grid error compensation approach was devised to overcome the basis mismatch. Specifically, we perform first-order Taylor expansion on the ideal steering vector $\boldsymbol{a}(\theta_k)$ of the interpolated virtual array:

$$\boldsymbol{a}(\theta_k) \approx \boldsymbol{a}\left(\hat{\theta}_k^l\right) + \boldsymbol{b}\left(\hat{\theta}_k^l\right)\gamma^l \tag{17}$$

where θ_k and $\hat{\theta}_k^l$ are the genuine incident direction and initial estimated DOA, respectively. The values $\boldsymbol{b}\left(\hat{\theta}_k^l\right) = \partial \boldsymbol{a}\left(\hat{\theta}_k^l\right) \Big/ \partial \hat{\theta}_k^l$ and $\gamma^l = \theta_k - \hat{\theta}_k^l$ are the initial off-grid errors. The eigen-decomposition of $\boldsymbol{R}(\hat{\boldsymbol{z}})$ is given by $\boldsymbol{R}(\hat{\boldsymbol{z}}) = \boldsymbol{U\Sigma U^{H}}$. Next, define noise subspace $\hat{\boldsymbol{E}}_n$, which consists of K columns of $\boldsymbol{U}$ corresponding to the K largest eigenvalues. According to the orthogonal property between $\hat{\boldsymbol{E}}_n$ and $\boldsymbol{a}(\theta_k)$ [21], we designed an optimization problem to calculate the off-grid error γ^l, which can be formulated as

$$\begin{aligned} \hat{\gamma}^l &= \arg\min_{\gamma^l} h\left(\gamma^l\right) = \arg\min_{\gamma^l} \left\| \hat{\boldsymbol{E}}_n^H \boldsymbol{a}(\theta_k) \right\|_2^2 \\ &= \arg\min_{\gamma^l} \left\| \hat{\boldsymbol{E}}_n^H \left[\boldsymbol{a}\left(\hat{\theta}_k^l\right) + \boldsymbol{b}\left(\hat{\theta}_k^l\right)\gamma^l \right] \right\|_2^2 \end{aligned} \tag{18}$$

The objective function $h\left(\gamma^l\right)$ can be simplified as

$$h\left(\gamma^l\right) = \varsigma_2^l (\gamma^l)^2 + \varsigma_1^l \gamma^l + \varsigma_0^l \tag{19}$$

where $\varsigma_2^l = \boldsymbol{b}^H\left(\hat{\theta}_k^l\right) \hat{\boldsymbol{E}}_n \hat{E}_n^H \boldsymbol{b}\left(\hat{\theta}_k^l\right) = \left\| \hat{\boldsymbol{E}}_n^H \boldsymbol{b}\left(\hat{\theta}_k^l\right) \right\|_2^2$, $\varsigma_1^l = 2\Re\left\{ \boldsymbol{a}^H\left(\hat{\theta}_k^l\right) \hat{\boldsymbol{E}}_n \hat{\boldsymbol{E}}_n^H \boldsymbol{b}^H\left(\hat{\theta}_k^l\right) \right\}$ and $\varsigma_0^l = \boldsymbol{a}^H\left(\hat{\theta}_k^l\right) \hat{\boldsymbol{E}}_n \hat{\boldsymbol{E}}_n^H \boldsymbol{a}\left(\hat{\theta}_k^l\right) = \left\| \hat{\boldsymbol{E}}_n^H a\left(\hat{\theta}_k^l\right) \right\|_2^2$. It is worth noting that $h\left(\gamma^l\right)$ is a quadratic function and $\varsigma_2^l > 0$, hence the optimal value of γ^l can be achieved by

$$\hat{\gamma}^l = -\frac{\varsigma_1^l}{2\varsigma_2^l} \tag{20}$$

Based on this, the DOA after the off-grid error compensation is

$$\hat{\theta}_k^{l+1} = \hat{\gamma}^l + \hat{\theta}_k^l \tag{21}$$

By repeating steps (20) and (21), the estimated DOA will be closer to the true value, hence a more accurate estimation result can be obtained.

3.4. Performance Analysis

Through array interpolation technology, the maximum aperture $|S_I|d$ and DOF provided by the virtual array are fully utilized in the proposed framework. For the extended coprime array shown in Figure 1, the maximum achievable DOF of our method is $2M_1M_2 - M_2$, which means that the proposed algorithm can identify a spatial direction of $2M_1M_2 - M_2$ GNSS signals. According to [22], our method is able to achieve higher resolution and accuracy since all elements and the maximum aperture of the derived virtual array are exploited for parameter estimation. In addition, we further improved the accuracy of DOA estimation by designing an optimization problem to compensate for the off-grid error caused by the virtual signal-sparse reconstruction.

Although better DOA estimation performance can be achieved by combining virtual array interpolation and error compensation, it comes with an increase in computational complexity in the algorithm. Compared with existing methods in [6,8,12], the additional computation introduced in our approach mainly focuses on three operations: virtual array interpolation, signal-sparse reconstruction and off-grid error compensation. Virtual array interpolation technology needs to recover the Toeplitz covariance matrix, and its computational complexity is $\mathcal{O}\left((2M_1M_2 - M_2 + 1)^3\right)$. Suppose the number of predefined spatial discrete grids is G, the computational costs required for signal-sparse reconstruction is $\mathcal{O}(G(2M_1M_2 - M_2 + 1))$. The main calculation amount of the error compensation unit is concentrated on the decomposition of the covariance matrix; thus, the computational complexity of the main calculation amount is approximately $\mathcal{O}\left((2M_1M_2 - M_2 + 1)^3\right)$.

4. Simulation Results

In this section, we give numerical examples to verify the performance of the proposed DOA estimation frame under a spoofing attack. Let the symbols SNRsp and SNRau denote the signal-to-noise ratio of the spoofing and the authentic signals, respectively. The settings of the basic simulation parameters are shown in Table 1. It is worth noting that the value of SNRsp and N are allowed to change in different simulation scenarios.

Table 1. Summary for simulation parameters.

Parameter	Setting
Intermediate frequency	4.092 MHz
Sampling frequency	37.851 MHz
Data length	20 ms
Samples in each chip	37
SNRau	−20 dB
Noise bandwidth	2 MHz
Regularization parameter	1
Predefined grid interval	1°
Maximum iteration number	1000
Extended coprime array	$M_1 = 3$, $M_2 = 5$

Specifically, we compared our method with the ULA-based Cyclic-MUSIC algorithm [6], the ULA-based MMUSIC algorithm [8] and the coprime array-based MMUSIC algorithm [12]. It can be seen from Table 1 that the extended coprime array consisted of $2M_1 + M_2 - 1 = 10$ sensors in total. For a fair comparison, the number of physical sensors in ULA was also set to ten. In the following subsections, we indicate the advantages of the proposed technique from three aspects: DOF enhancement, resolution and accuracy.

4.1. DOF Comparison

In this experiment, we assumed that the pseudo random noise (PRN) code and DOA of the incident sources were as shown in Table 2. The SNRsp was set to be −17 dB and the parameter N = 37,000. The DOF comparison results are shown in Figure 3. It can be seen from Table 2 that the number of incident sources was $K = 17$, which exceeds the maximum achievable DOFs of the ULA-based Cyclic-MUSIC algorithm and the ULA-based MMUSIC algorithm, as well as the coprime array-based MMUSIC algorithm. In this case, all algorithms used for comparison except the proposed method were invalid. Thus, Figure 3 contains only the results of the proposed algorithm. As Figure 3 shows, our approach could effectively estimate all of the seventeen sources. Consequently, it is obvious that the enhanced DOFs could be obtained by the proposed frame.

Table 2. Simulation parameters of incident sources in Section 4.1.

	Sat1	Sat2	Sat3	Sat4	Sat5	Sat6	Sat7	Sat8	Sat9	Sat10	Sat11	Sat12	Sat13	Sat14	Sat15	Sat16	Spoofing
PRN	2	3	5	6	8	10	12	13	15	16	18	19	21	22	26	29	[2,5,8,19,26]
DOA	−65°	−60°	−50°	−40°	−30°	−20°	−10°	−5°	5°	10°	20°	30°	40°	50°	60°	65°	0°

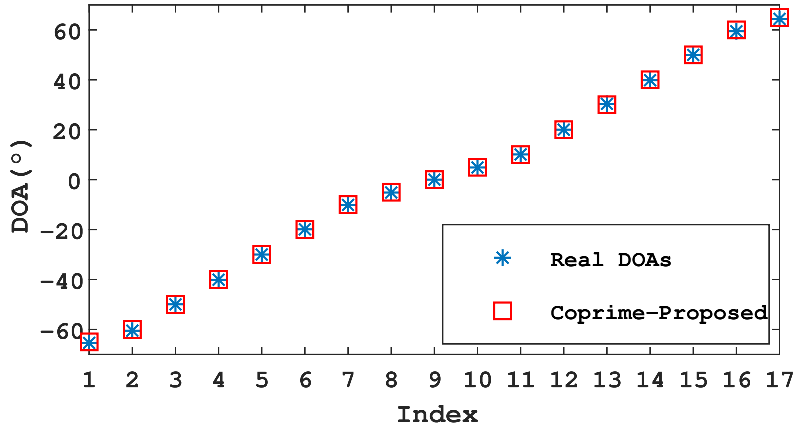

Figure 3. DOF comparison results.

4.2. Resolution Comparison

In this simulation, we compared the resolution by assuming two closely spaced sources: a satellite signal and a spoofing source. The parameters of the incident signals are shown in Table 3. Here, the SNRsp was −18 dB and $N = 37{,}000$. The resolution comparison results are displayed in Figure 4. It can be observed from Figure 4b that the spatial spectrum of both the ULA-based Cyclic-MUSIC algorithm and the ULA-based MMUSIC algorithm have only one peak; that is, they failed to identify the two closely spaced sources. Although the coprime array-based MMUSIC algorithm is capable of forming two peaks, its results deviated from the actual directions. In contrast, the result in Figure 4a indicates that the proposed algorithm is able to accurately estimate two closely spaced directions. Therefore, the proposed algorithm achieved better resolution of DOA estimation. The reason for this result is that the proposed algorithm could provide larger aperture through its array interpolation step.

Table 3. Simulation parameters of incident sources in Section 4.2.

	Sat1	Spoofing
PRN	1	[1,2,22,25]
DOA	−1°	1°

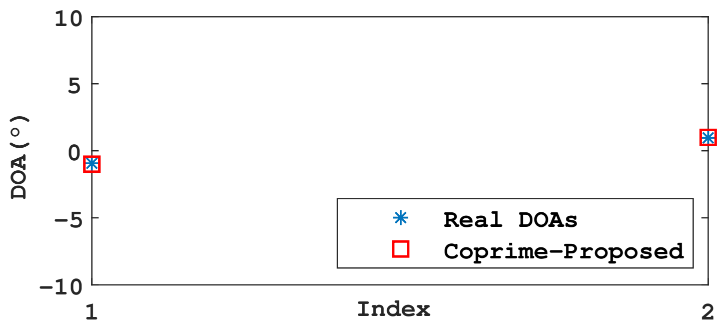

(**a**)

Figure 4. *Cont.*

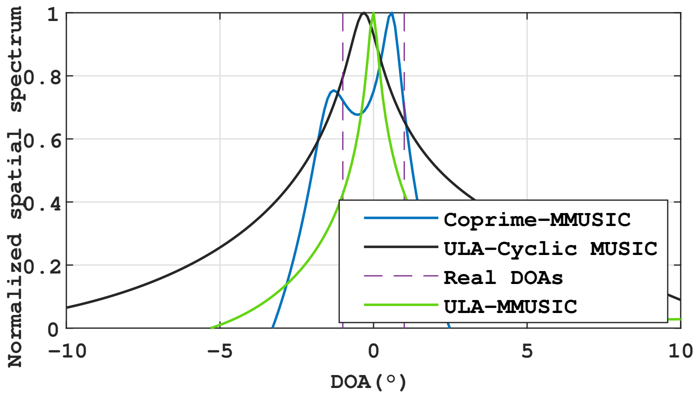

(**b**)

Figure 4. Resolution comparison results. (**a**) The proposed method; (**b**) ULA-based Cyclic-MUSIC algorithm, ULA-based MMUSIC algorithm and coprime-based MMUSIC algorithm.

4.3. Accuracy Comparison

In the last example, we conducted Monte Carlo simulations to compare the accuracy of three algorithms with root mean square error (RMSE). The RMSE can be expressed as

$$\mathrm{RMSE} = \sqrt{\frac{1}{QK}\sum_{q=1}^{Q}\sum_{k=1}^{K}\left(\hat{\theta}_{k,q} - \theta_k\right)^2} \tag{22}$$

where $\hat{\theta}_{k,q}$ is the DOA estimation result of the k-th source in the q-th Monte Carlo trial and θ_k denotes the real DOA of the k-th source. We assume $Q = 1000$ in this subsection.

Table 4 shows the relevant parameters of incident sources. The accuracy comparison results are plotted in Figure 5. In Figure 5a, we fixed SNRsp = −17 dB and varied N from 500 to 5000. We can see from Figure 5a that the RMSE of all the algorithms decreased with the increase in N, where the proposed method had lower RMSE compared with other algorithms. This demonstrated that the combination of array interpolation and off-grid error compensation can produce more accurately estimated results, especially when the N is finite. In addition, as shown in Figure 5a, when N was greater than 1500, the RMSE of the proposed algorithm decreased slowly as the theoretical accuracy of the proposed algorithm was limited by the Cramer–Rao bound (CRB). The CRB of DOA estimation is not only related to the number of samples N, but it is also affected by various parameters, such as the number of incident signals, array structure, the number of sensors in array and so forth [22]. Therefore, under the condition of the same incident signals, the RMSE of our algorithm and the coprime array-based MMUSIC algorithm had a similar change curve, owing to the same array configuration. We next fixed $N = 37{,}000$ when the SNRsp varied between −25 dB and −17 dB, this is shown in Figure 5b. We can observe in Figure 5b that our approach is superior to the other three algorithms in the whole SNRsp range. Moreover, the RMSE of all algorithms remained almost unchanged with the increase in the power of spoofing.

Table 4. Simulation parameters of incident sources in Section 4.3.

	Sat1	**Sat2**	**Sat3**	**Sat4**	**Spoofing**
PRN	2	5	8	19	[2, 5, 8, 19]
DOA	−40°	−27°	−3°	28°	12°

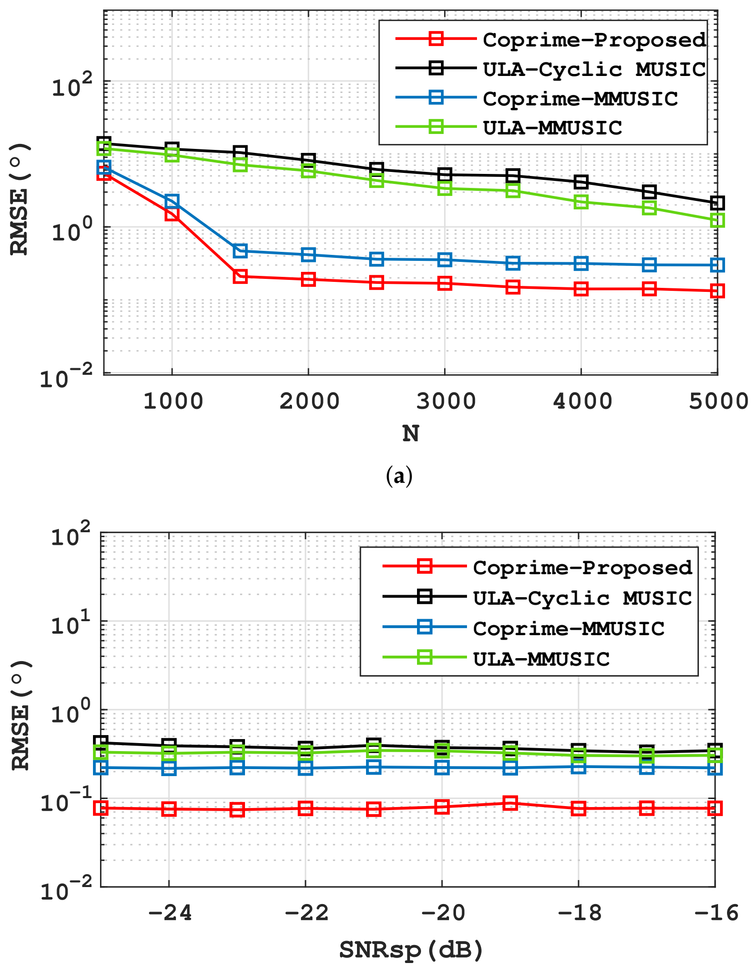

Figure 5. Accuracy comparison results. (**a**) RMSE versus N; (**b**) RMSE versus SNRsp.

5. Conclusions

In this paper, we proposed a novel DOA estimation scheme under a GNSS spoofing attack using a coprime array of antennas. We first constructed a denoised covariance matrix to achieve DOA estimation before receiver despreading. Then, we derived the virtual ULA through the array interpolation technique to fully utilize the maximum aperture provided by the virtual array. Based on this, the sparse reconstruction method based on off-grid error compensation was designed to solve the basis mismatch. Finally, simulation results indicated the superiority of our DOA estimation approach in DOFs, resolution and accuracy.

Although the proposed DOA estimation method showed performance advantages under a spoofing attack, it may fail in a multipath environment and small time-offset spoofing scenarios due to the increased correlation between incident signals. Given this problem, it is necessary to further explore the de-correlation DOA estimation algorithm to cope with a multipath environment and small time-offset spoofing. Moreover, we plan to develop deterministic analysis on the performance of the DOA estimation method based on a coprime array in GNSS, and we will attempt to give the closed-form solution for resolution, bias and CRB.

Author Contributions: Conceptualization, F.S. and Y.Z.; methodology, Y.Z. and B.Q.; software, Z.M.; validation, Z.M. and Y.Z.; formal analysis, Y.Z.; investigation, Y.Z.; data curation, B.Q.; writing—original draft preparation, Y.Z.; writing—review and editing, Y.Z.; funding acquisition, F.S. All authors have read and agreed to the published version of the manuscript.

Funding: This research was funded by the National Natural Science Foundation of China, grant number 61673128 and 61573117.

Data Availability Statement: Not applicable.

Conflicts of Interest: The authors declare no conflict of interest.

References

1. Wei, X.; Wang, Y.; Sun, C. PerDet: Machine-Learning-Based UAV GPS Spoofing Detection Using Perception Data. *Remote Sens.* **2022**, *14*, 4925. [CrossRef]
2. Psiaki, M.L.; Humphreys, T.E. GNSS Spoofing and Detection. *Proc. IEEE* **2016**, *104*, 1258–1270. [CrossRef]
3. Meng, L.; Yang, L.; Yang, W.; Zhang, L. A Survey of GNSS Spoofing and Anti-Spoofing Technology. *Remote Sens.* **2022**, *14*, 4826. [CrossRef]
4. Broumandan, A.; Jafarnia-Jahromi, A.; Daneshmand, S.; Lachapelle, G. Overview of Spatial Processing Approaches for GNSS Structural Interference Detection and Mitigation. *Proc. IEEE* **2016**, *104*, 1246–1257. [CrossRef]
5. Jain, H.; Lo, S.; Chen, Y.H.; Rothmaier, F.; Powell, J.D. Accommodating direction ambiguities in direction of arrival based gnss spoof detection. In Proceedings of the ION 2019 Pacific PNT Meeting, Honolulu, HI, USA, 8–11 April 2019; pp. 274–289.
6. Zhang, J.; Cui, X.; Xu, H.; Lu, M. A two-stage interference suppression scheme based on antenna array for GNSS jamming and spoofing. *Sensors* **2019**, *19*, 3870. [CrossRef]
7. Appel, M.; Konovaltsev, A.; Meurer, M. Robust spoofing detection and mitigation based on direction of arrival estimation. In Proceedings of the 28th International Technical Meeting of The Satellite Division of the Institute of Navigation (ION GNSS+ 2015), Dana Point, CA, USA, 26–28 January 2015; pp. 3335–3344.
8. Xu, G.; Shen, F.; Amin, M.; Wang, C. DOA classification and CCPM-PC based GNSS spoofing detection technique. In Proceedings of the 2018 IEEE/ION Position, Location and Navigation Symposium (PLANS), Monterey, CA, USA, 23–26 April 2018; pp. 389–396.
9. Shi, J.; Wen, F.; Liu, Y.; Liu, Z.; Hu, P. Enhanced and Generalized Coprime Array for Direction of Arrival Estimation. *IEEE Trans. Aerosp. Electron. Syst.* **2022**, 1–12. [CrossRef]
10. Zhang, L.; Wang, H.; Wen, F.Q.; Shi, J.P. PARAFAC Estimators for Coherent Targets in EMVS-MIMO Radar with Arbitrary Geometry. *Remote Sens.* **2022**, *14*, 2905. [CrossRef]
11. Wen, F.; Shi, J.; He, J.; Truong, T.K. 2D-DOD and 2D-DOA Estimation Using Sparse L-Shaped EMVS-MIMO Radar. *IEEE Trans. Aerosp. Electron. Syst.* **2022**, 1–7. [CrossRef]
12. Zhao, Y.; Shen, F.; Zhou, D. A Spoofing Detection Algorithm Based on Coprime Array for GNSS Receiver. In Proceedings of the China Satellite Navigation Conference (CSNC 2021) Proceedings, Nanchang, China, 22–25 May 2021; pp. 387–396.
13. Pal, P.; Vaidyanathan, P.P. A Grid-Less Approach to Underdetermined Direction of Arrival Estimation via Low Rank Matrix Denoising. *IEEE Signal Process. Lett.* **2014**, *21*, 737–741. [CrossRef]
14. Qi, B.; Wang, W.; Wang, B. Off-Grid Compressive Channel Estimation for mm-Wave Massive MIMO with Hybrid Precoding. *IEEE Commun. Lett.* **2019**, *23*, 108–111. [CrossRef]
15. Amin, M.; Sun, W. A novel interference suppression scheme for global navigation satellite systems using antenna array. *IEEE J. Sel. Areas Commun.* **2005**, *23*, 999–1012. [CrossRef]
16. Sun, W.; Amin, M.G. A self-coherence anti-jamming GPS receiver. *IEEE Trans. Signal Process.* **2005**, *53*, 3910–3915. [CrossRef]
17. Kou, J.; Li, M.; Jiang, C. Robust Direction-of-Arrival Estimation for Coprime Array in the Presence of Miscalibrated Sensors. *IEEE Access* **2020**, *8*, 27152–27162. [CrossRef]
18. Fan, X.; Zhou, C.; Gu, Y.; Shi, Z. Toeplitz Matrix Reconstruction of Interpolated Coprime Virtual Array for DOA Estimation. In Proceedings of the 2017 IEEE 85th Vehicular Technology Conference (VTC Spring), Sydney, Australia, 4–7 June 2017; pp. 1–5.
19. Paik, J.W.; Hong, W.; Lee, J.H. Direction-of-Departure and Direction-of-Arrival Estimation Algorithm Based on Compressive Sensing: Data Fitting. *Remote Sens.* **2020**, *12*, 2773. [CrossRef]
20. Luo, J.; Zhang, Y.; Yang, J.; Zhang, D.; Zhang, Y.; Zhang, Y.; Huang, Y.; Jakobsson, A. Online Sparse DOA Estimation Based on Sub–Aperture Recursive LASSO for TDM–MIMO Radar. *Remote Sens.* **2022**, *14*, 2133. [CrossRef]
21. McCloud, M.; Scharf, L. A new subspace identification algorithm for high-resolution DOA estimation. *IEEE Trans. Antennas Propag.* **2002**, *50*, 1382–1390. [CrossRef]
22. Zhou, C.; Gu, Y.; Fan, X.; Shi, Z.; Mao, G.; Zhang, Y.D. Direction-of-Arrival Estimation for Coprime Array via Virtual Array Interpolation. *IEEE Trans. Signal Process.* **2018**, *66*, 5956–5971. [CrossRef]